Radiation Physics and Chemistry 177 (2020) 109107

Contents lists available at ScienceDirect

Radiation Physics and Chemistry

journal homepage: www.elsevier.com/locate/radphyschem

Study of Fe ions in aquamarine and the effect of dichroism as seen using UV–Vis, NIR and x-ray

Nantharat Bunnag[a], Bootsaba Kasri[a], Watcharakon Setwong[b], Ekkasit Sirisurawong[c], Maneerat Chotsawat[c], Prae Chirawatkul[c], Chatree Saiyasombat[c,*]

[a] Faculty of Gems, Burapha University, Chanthaburi Campus., Chanthaburi, 22170, Thailand
[b] School of Chemistry, Suranaree University of Technology, Nakhon Ratchasima, 30000, Thailand
[c] Synchrotron Light Research Institute (Public Organization), Nakhon Ratchasima, 30000, Thailand

ARTICLE INFO

Keywords:
X-ray absorption
XANES
Aquamarine
Orientation
Dichroism

ABSTRACT

The oxidation states and coordination environment of Fe in 4 aquamarine samples with different color shades were studied. The C axis along with plane A and plane C of the samples were identified and the measurements were made with plane A oriented facing incoming beam and plane C oriented facing incoming beam. NIR and Raman spectroscopy were employed to confirm the structure of the samples. XRD was used to confirm the polished faces. UV–Vis and X-ray absorption near edge structure (XANES) were used to identify the presence of both Fe^{2+} and Fe^{3+} in the samples. The results indicated that Fe resided predominantly in 6-fold coordinated sites and the deep blue shade depended on the amount of Fe^{2+} in 6-fold coordinated sites. The effect of dichroism was noticeable in NIR, Raman spectroscopy, UV–Vis and XANES. Clearer Raman bands were observed when samples were oriented with plane A facing laser source. NIR and UV–Vis analysis could benefit from the complementarity of spectra measured from both orientations. Discrepancies between XANES spectra measured from the two orientations could lead to uncertainties in obtained values of oxidation states.

1. Introduction

Gemstones are natural inorganic materials with physical features such as their lusters and colors which considered high aesthetic value. They are also durable which make them practical ornament pieces in various jewelry. Some gemstones are rare which puts them on high demands thus high commercial values. As price of gemstones markedly depends on their types and colors. The origins of colors in various gemstones were extensively studied.

Aquamarine is one of the important gemstones because of its rarity especially the deep blue color aquamarines which are most valuable. Aquamarines belong to a beryl mineral family ($Be_3Al_2Si_6O_{18}$) and a soft texture gemstone group with a hexagonal crystal system. Beryl can be found in many colors and often named after their colors, including emerald (green), aquamarine (blue-green), morganite (pink), and heliodor (yellow). The structure of beryl consists of layers of cyclic silicates Si_6O_{18} connected to Al^{3+} forming octahedral sites and connected to Be^{2+} forming tetrahedron sites as shown in Fig. 1. The layers of cyclic silicates are stacked along the C axis (optical axis) creating channels which are often filled by water (type I H_2O and type II H_2O), carbon dioxide, or alkali ions (Deer et al., 1997). The cations can also be found in 6-fold coordinated interstitial sites located between two octahedral sites along the C axis.

Color variation in beryl has been extensively theorized. The common conclusion involved transition metals replacing Al^{3+} in octahedral sites or transition metals filling channel sites. It has been reported that the blue color of aquamarine originated from the presence of Fe^{2+} in channel sites (Goldman et al., 1978). Wood and Nassau (1968) and Adamo et al. (2008) reported that V^{3+} replacing Al^{3+} in octahedral sites caused green color, Cr^{3+} replacing Al^{3+} caused intense green color, and that beryl became colorless when Fe^{2+} replaced Al^{3+}. Deer et al., (1997) reported that Fe^{3+} replaced Al^{3+} also produced yellow beryl. Wood and Nassau (1968) found that pink beryl originated from Mn^{2+} replacing Al^{3+} together with Mn^{2+} filling channel sites. And when Al^{3+} was replaced by Mn^{3+} the color became red. In addition, Fe^{2+}/Fe^{3+} inter-valence charge transfer (IVCT) could produce intense blue (Taran and Rossman, 2001), O^{2-}/Fe^{3+} charge transfer could produce intense yellow (Fritsch and Rossman, 1988) and color center theory could be used to explain the deep blue shade (Nassau et al., 1976).

Dichroism in a gemstone as seen from visible light results in 4 types of refraction including single refraction, double refraction, aggregate or

* Corresponding author.
E-mail address: chatree@slri.or.th (C. Saiyasombat).

https://doi.org/10.1016/j.radphyschem.2020.109107
Received 25 February 2020; Received in revised form 22 June 2020; Accepted 10 July 2020
Available online 18 July 2020
0969-806X/

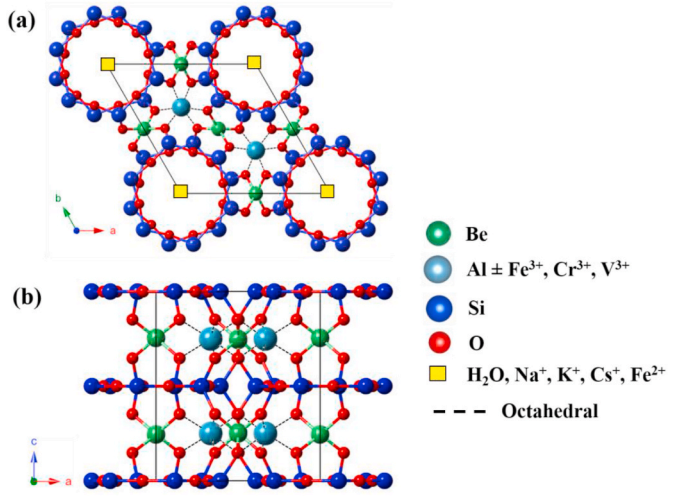

Fig. 1. Crystal structure of beryl ($Be_3Al_2Si_6O_{18}$) projected on (a) basal plane {0001} and (b) prismatic plane {1010}. The green, light blue, blue and red colors represent Be, Al, Si and O atoms, respectively. The unit cell is denoted by black lines. Dashed lines describe the octahedral sites which could also be occupied by other atoms such as Fe^{3+}, Cr^{3+} and V^{3+}. Ring channels on channel sites are shown by yellow squares which could be occupied by ions or molecules such as CO_2, H_2O, Na^+, K^+, Cs^+ and Fe^{2+}. (For interpretation of the references to color in this figure legend, the reader is referred to the Web version of this article.)

polycrystalline and anomalous double refraction. As beryl is hexagonal, it consists of 2 unequal axes and the refraction property is uniaxial double refraction. This means when the beam of light passes through the structure, it splits into two rays, ordinary and extraordinary rays. The effect of dichroism has also been reported for x-rays. Uniaxial minerals such as buergerite and scapolite and biaxial minerals such as epidote and fayalite showed different X-ray absorption near edge structure (XANES) spectra with respect to their orientations (Waychunas and Brown, 1990 and Dyar et al., 2002). As dichroism could lead to errors in data interpretation, its effect should be considered when optical or structural properties were determined using various techniques employing light across wavelengths.

In this work, oxidation states and coordination environments of Fe in aquamarine samples with different color shades were investigated. X-ray absorption spectroscopy (XAS) is a well-established analytical technique used extensively for understanding atomic local structure as well as electronic states. The technique is used to study oxidation states of transition metals as well as other impurity elements, symmetry surrounding probed elements, and neighboring environments such as coordination numbers and bond distances. The link between color and local structures of Fe could lead to insights into the gemstones' color and useful to gemstone treatment process improvement. The effects of dichroism to Ultraviolet–Visible spectroscopy (UV–Vis), Near infrared spectroscopy (NIR), Raman spectroscopy and XAS of aquamarine are discussed.

1.1. Experimental methods

Four aquamarine samples from Africa were selected: AQ01, AQ02-1, AQ02-2, and AQ03. All samples were of different color shades as shown in Fig. 2. AQ02-1 and AQ02-2 were cut from the same crystal to double check the method as they should produce similar results. C axes of all samples were identified using polarize scope before the samples were cut and polished. For AQ03, its natural faces were used as a guideline for polishing. Then, XRD was used to confirm obtained crystal planes of the samples related to their faces. X-ray data were collected with Rigaku SmartLab diffractometer in the range of 10–50 in 2θ by a step-scanning mode, with a step size of 0.02, and a count time of 10 s per step. The measurements were carried out with Cu-Kα radiation operating at 40 kV and 40 mA.

Raman spectroscopy measurements were performed using Bruker Senterra II spectrometer system. Peaks in Raman spectrum correspond to vibration frequencies of specific molecular bonds. This technique can be used to identify types of molecules and study chemical bonding and intramolecular bonds. Each sample was measured at 8 locations using a dispersive Raman microscope and averaged. Spectra were acquired with a laser wavelength of 532 nm, power of 50 mW, 50X magnification, and 10 repeated measurements were made for each position with 10 s exposure time.

UV–Vis–NIR spectrophotometer is an instrument which measures the intensity of light in the UV, visible and near-IR region that penetrates or is absorbed by samples. It can be used as a fingerprint to specify types and densities of compounds contained in samples. In this work, UV–Vis–NIR Spectra were recorded using PerkinElmer LAMBDA 950 which is a high-performance UV/Vis/NIR spectrophotometer employing deuterium and tungsten halogen light sources. UV–Vis–NIR spectra were measured in transmission set up with integrating spheres covering 250–2000 nm range. All measurements were taken at room temperature using unpolarized light sources.

XANES provides information about oxidation states, electronic structures, and symmetries of probed elements. Fe K-edge XANES spectra were recorded at BL1.1W MXT of the Synchrotron Light Research Institute (SLRI), Thailand. As Fe concentration in aquamarine is low, the measurements were made in fluorescence-mode using 19-element Ge detector. The X-ray aperture size was 3 mm × 4 mm. The face of samples were placed at an angle of 45° to both the incident beam and the fluorescence detector for measurements. Standard materials representing Fe^0, Fe^{2+} and Fe^{3+} including Fe foil, FeO and Fe_2O_3, were

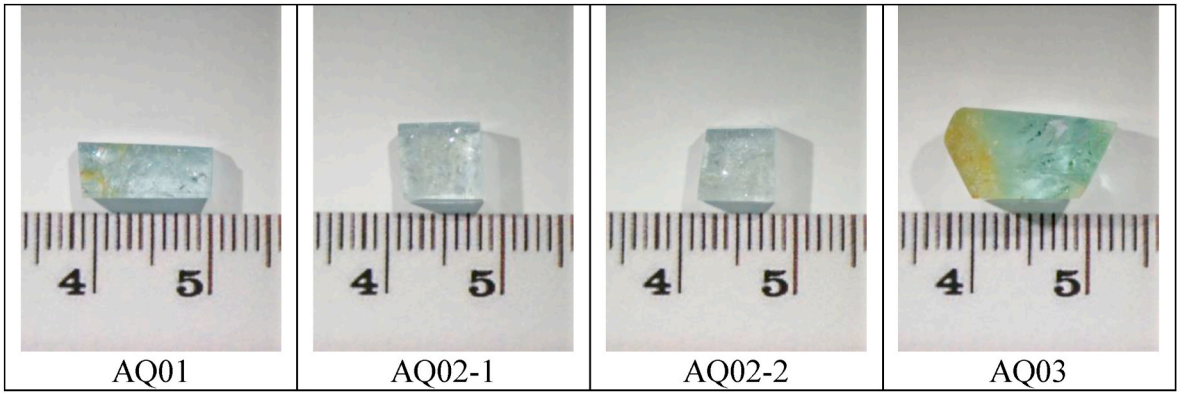

Fig. 2. Aquamarine samples with different color shades studied in this work. AQ01 is blue. AQ02-1 and AQ02-2 are light blue. And AQ03 is bluish green. (For interpretation of the references to color in this figure legend, the reader is referred to the Web version of this article.)

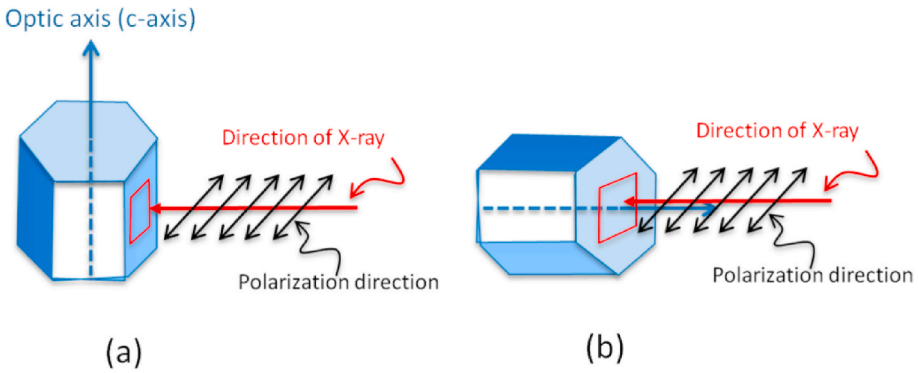

Fig. 3. Illustration of sample orientations, (a) with plane A facing incoming x-rays and (b) with plane C facing incoming x-rays.

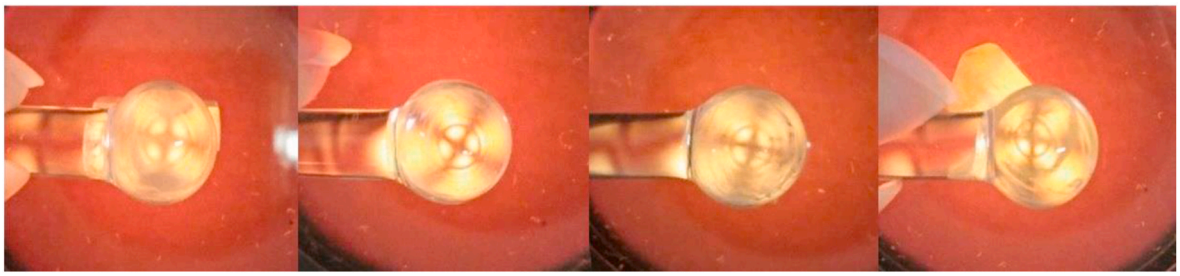

Fig. 4. Uniaxial double reflection of aquamarine samples as seen from a polarize scope. AQ01, AQ02-1, AQ02-2, and AQ03 are arranged from left to right.

measured in transmission mode. The ionization energy (E0) used was 7112 eV with a scan range from 150 eV below E0 to 200 eV above E0 and a collection time of 1 s per point.

From a preliminary test, the XANES spectra obtained from samples which were aligned with C axis parallel and perpendicular to the polarization of x-rays were similar. Noticeable changes could be observed when samples were aligned with C axis perpendicular to polarization but with plane A facing incoming x-rays and plane C facing incoming x-rays as shown in Fig. 3. Thus, all measurements were made according to these orientations.

2. Results and discussion

Double reflection was observed for all samples as shown in Fig. 4. The photographs were taken from a polarize scope and typical crosses on the plane C characteristic of uniaxial reflection confirmed the hexagonal structure of aquamarine and that plane C was correctly identified.

The XRD results are shown in Fig. 5. XRD patterns of beryl JCPDS-00-009-0430 was used as a reference pattern. The XRD patterns measured with plane A facing x-rays contained the expected peaks at 10.96° and 11.02° for AQ01 and AQ03, respectively, corresponding to the (100) plane. For measurements with plane C facing x-rays, AQ01 and AQ03 patterns contained the peaks at 19.40° and 19.26°, respectively, corresponding to the (001) plane. The XRD results confirmed that the aquamarine faces of AQ01 and AQ03 were correctly polished to plane A and plane C. The XRD patterns from AQ02-1 and AQ02-2 could not be determined, although the polished planes were implied from the uniaxial double reflection seen from the polarized scope.

The Raman results are shown in Fig. 6. Raman bands corresponding to bond vibration in the beryl structure were observed in all samples. The reported Raman bands for beryl are shown in Table 1 (Adams and Gardner, 1974; Prencipe and Nestola, 2007; O'Bannon and Williams, 2016) and CO_2 (Charoy et al., 1996).

The effect of dichroism observed for all samples was the same. The intensity of the bands at 323 and 1068 cm^{-1} was stronger when plane A was oriented facing laser. The intensity of the band at 397 cm^{-1}, on

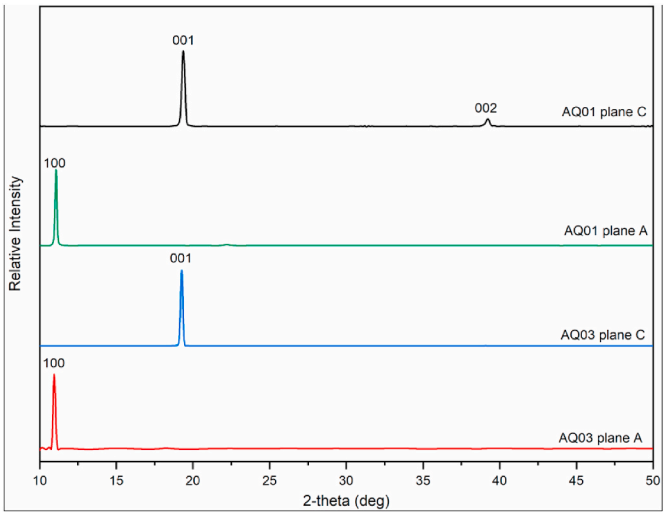

Fig. 5. XRD patterns of aquamarine samples AQ01 and AQ03. Measurements were made with plane A facing x-rays and plane C facing x-rays.

the other hand, was stronger when plane C was oriented facing laser while the intensity of the band at 686 cm^{-1} remained invariant. The band at 1010 cm^{-1} was observed shifted to lower wavevector when plane C was oriented facing laser.

Detail of atomic motions involved in all possible vibrational modes of beryl could be found elsewhere, for example, at the CRYSTAL website.[1] The discussion here is limited to A_{1g} mode corresponding to the observed prominent bands at 323, 397, 686, 1068 cm^{-1} in the measured range of 200–1400 cm^{-1}. The A_{1g} mode involves motions of atoms in the cyclic silicates rings which consists of connected Si-centered tetrahedra arrange in 6-fold symmetry. Each band corresponds to different vibrations of the structure, for example, the band at 323 cm^{-1}

[1] http://www.crystal.unito.it/vibs/beryl.

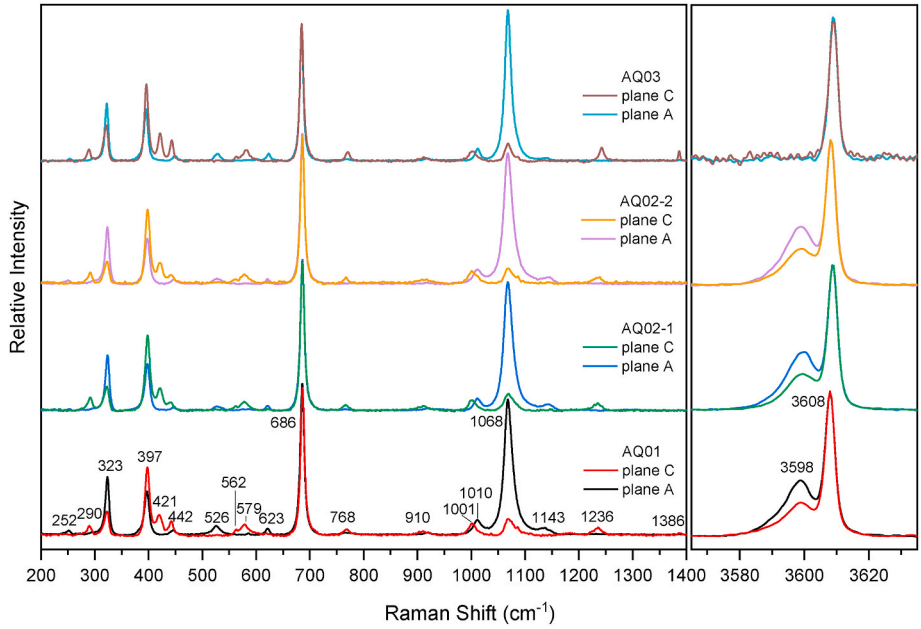

Fig. 6. Raman spectra of aquamarine samples AQ01, AQ02-1, AQ02-2, and AQ03 oriented with plane A facing laser source and plane C facing laser source. The measurements were made in the ranges 200-1400 cm^{-1} and 3565-3635 cm^{-1}.

corresponds to the bending of the Si–O–Si bond angle between Si-centered tetrahedra, whereas the band at 397 cm^{-1} corresponds to the bending of the angle between Si, Be and Al-centered polyhedra (Kim et al., 1995). The observed enhanced peak intensity due to dichroism could be explained considering positions of the involved atoms. The bands at 1236 and 1386 cm^{-1} are related to the vibration of CO_2 in the channel site (Charoy et al., 1996). The bands could only be seen when plane C was oriented facing laser because the only possible orientation of CO_2 in the channel sites is aligned parallel to the c-axis.

The measurements in the 3500-3700 cm^{-1} range gave information regarding the type of water molecules in channel sites (Aurisicchio et al., 1988; Sherriff et al., 1991). As seen in Fig. 6, only AQ01, AQ02-1 and AQ02-2 showed two types of water molecules, type-I H_2O and type-II H_2O, with a greater amount of type-I H_2O as seen from a stronger intensity of the band at 3608 cm^{-1}. This agreed with a suggestion made by Charoy et al. (1996) that channel sites contained a high content of type-I H_2O and a small content of alkali. Only the intensity of the band at 3598 cm^{-1} corresponding to type-II H_2O showed variation due to dichroism. As the interpretation of Raman spectroscopy for these samples can be made qualitatively by fingerprinting the band positions, measurements with plane A oriented facing laser gave overall clearer band positions, especially detection of type-II H_2O molecules and deformation of O_2–Al/Be–O_2.

The NIR absorption spectra of the samples in the range from 1000 nm to 2000 nm are shown in Fig. 7. The spectra contained two main bands at 1410 nm and 1895 nm. Reported band positions found in the beryl structure are presented in Table 2. As seen from the table, most observable bands corresponded to vibrations involving type-I H_2O and only the band at 1895 nm involved type-II H_2O. Due to Coulomb interaction between cations in the channel sites, water molecules are oriented two ways, 90° relative to each other, defined as type-I and type-II. This different orientations along with their weak Van der Waals interaction to the channel walls results in an anisotropic effect on the vibration of the incoming light (Zhukova et al., 2014). Unlike Raman results, type-II H_2O in AQ03 was detectable as seen from the presence of the band at 1895 nm although the intensity of the band was considerably less than those of AQ01, AQ02-1 and AQ02-2 which is in agreement with the Raman result. The effect of dichroism for NIR spectra was similar for all samples. The intensity of the band at 1837 cm^{-1} was stronger when plane C was oriented facing IR whereas the intensity of the bands at 1410 cm^{-1} and 1962 cm^{-1} were stronger when plane A was oriented facing IR. For NIR spectroscopy, the measurements of the two orientations gave complementary focuses of

Table 1
Reported Raman bands expected in the spectra of aquamarine (Adams and Gardner, 1974; Prencipe and Nestola, 2007; O'Bannon and Williams, 2016, Charoy et al., 1996).

Band position (cm^{-1})	Assignment
290	Ring vibration
323	Ring and Al distortion or ring vibration
397	Ring breathing
526	Si and Be bending or Al–O vibration
686	Be–O stretch or Si–O–Si stretch
1010, 1068	Si–O_2 stretch and O_2–Al/Be–O_2 deformation
1236, 1386	CO_2
3598	OH-stretch of type-II H_2O
3608	OH-stretch of type-I H_2O

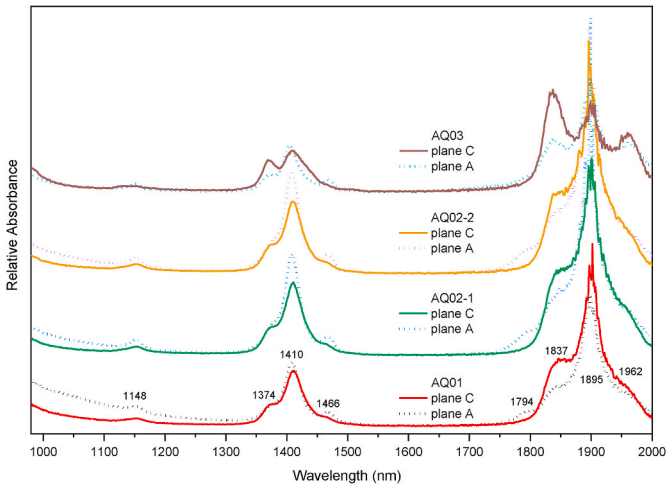

Fig. 7. NIR spectra of aquamarine samples AQ01, AQ02-1, AQ02-2, and AQ03 measured with plane A and plane C facing IR.

Table 2
Reported NIR peaks of aquamarine (Hunt and Salisbury, 1970; Wood and Nassau, 1967).

Band position (nm)	Assignment
1148	ν_1, ν_2 and ν_3 mode of type-I H_2O molecule.
1374	ν_1 and ν_3 vibration of type-I H_2O molecule
1410	ν_1 and ν_3 mode of type-I H_2O molecule.
1466	$2\nu_2$ and ν_3 mode of type-I H_2O molecule
1794	–
1837	ν_2 and ν_3 mode of type-I H_2O molecule
1895	ν_2 and ν_3 mode of type-II H_2O molecule
1962	ν_2 and ν_3 mode of type-I H_2O molecule

spectral features and it would be useful to compare them.

The UV–Vis spectra of the samples contained three main absorption peaks at 373, 428 and 825 nm, as shown in Fig. 8. It has been reported that the peak at 825 nm was related to either Fe^{2+} in octahedral site or Fe^{2+} in channel site and the peaks at 373 and 428 nm were assigned to Fe^{3+} in octahedral sites as suggested by Wood and Nassau (1968); Goldman et al., (1978); Taran and Rossman, 2001; Chankhantha et al., (2016) or in octahedral sites, channel site or interstitial sites as suggested by Spinolo et al., (2007). The spectra measured with plane C oriented facing light source showed clearer peaks for all three peaks in all samples. However, for AQ03, a peak shoulder around 700 nm was observed when plane A was oriented facing light source.

The peak shoulder at 700 nm relates to the amount of Fe^{2+} in the octahedral site. Parkin et al. (1977) proposed that the peak shoulder at 700 nm originated from IVCT between Fe^{2+} in the octahedral site and Fe^{3+} in adjacent octahedral sites along the C axis which produced deep blue shade. Goldman et al. (1978), on the other hand, proposed that the peak shoulder originated from either the interaction between Fe^{2+} and Fe^{3+} in channel sites along the C axis or the interaction between Fe^{2+} in octahedral sites and Fe^{3+} in the interstitial site immediately adjacent between two octahedral sites along the C axis. It has been observed that many pale aquamarines have little or no absorption at 700 nm which suggested that the peak shoulder at 700 nm related to Fe^{2+}/Fe^{3+} IVCT between Fe^{3+} and Fe^{2+}. Therefore, the absence or weakness of peak shoulders at 700 nm found for the samples in this work could relate to their pale shades and suggested that not all Fe ions reside in octahedral sites. The spectrum of AQ03 measured with plane A oriented facing light source was the only spectrum that contained this feature and it was the sample which had the most intense blue shade of all the samples.

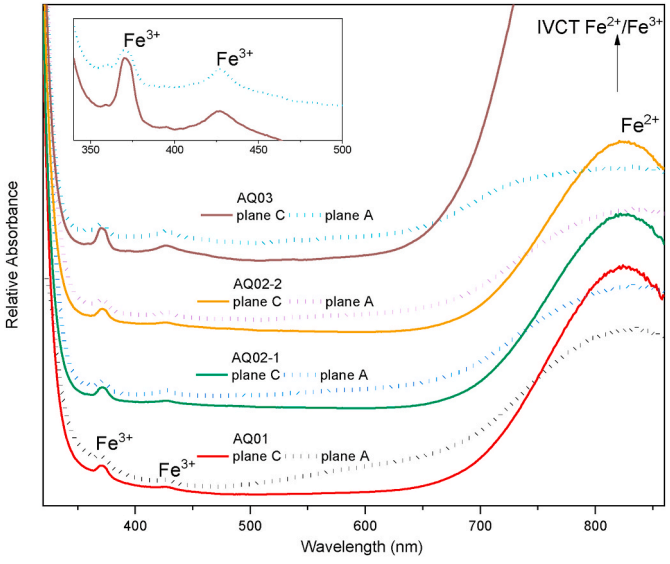

Fig. 8. UV–Vis spectra of aquamarine samples AQ01, AQ02-1, AQ02-2, and AQ03 measured with plane A facing light source and plane C facing light source. The inset shows a focus range between 320 nm and 500 nm of AQ03 sample.

As the main peaks in the UV–Vis spectra could be clearly observed when samples were oriented with plane C facing light source, the peak at 825 nm could dominate the shoulder feature at 700 nm. For this reason, the spectra where samples were oriented with plane A facing light source could also be useful in observing a peak shoulder at 700 nm.

We employed synchrotron XAS techniques to investigate the oxidation state and local environments of Fe atoms in the samples. XANES spectra for samples oriented with plane A facing x-rays and plane C facing x-rays are plotted together with those of standards and shown in Fig. 9. From the figure, the most prominent feature around the absorption edge region is **c** for AQ01 and **d** for AQ02-1, AQ02-2 and AQ03. A similar trend was observed for spectra corresponding to samples oriented with plane A facing x-rays (dotted lines) and those with plane C facing x-rays (solid lines). Spectra corresponding to AQ02-1 and AQ02-2 were the same.

The spectral features at position **a**, or pre-edge, corresponds to the electronic transition from 1s to 3d orbitals. Although the transition is spin-forbidden, site asymmetry could promote 3d and 4p mixing in Fe which results in non-zero probability for 1s to 3d transitions and the pre-edge feature (Waychunas et al., 1989). Site symmetry of Fe could thus be evaluated from the characteristic of pre-edge features. Pre-edge fit used for site symmetry determination of various coordination environments and their Fe oxidation state has been demonstrated (Wilke et al., 2001). Following the method employed by Wilke et al., (2001), a summary of pre-edge parameters determined for all samples in this work is shown in Fig. 10. The parameters from the pre-edge fit indicated that Fe ions in all samples were predominantly 6-fold coordinated but a distribution of ratios between Fe^{2+} and Fe^{3+} were observed. Although there are two 6-fold coordinated sites in beryl structure, the octahedral sites of Al^{3+} and the trigonal prismatic sites of the interstitial position between two Al^{3+} sites along the c-axis, the differentiation between these sites could not be made using this method.

The effect of dichroism provided uncertainties to the determined oxidation states. For AQ01 and AQ02, a slightly larger amount of Fe^{3+} was implied when plane A was oriented facing x-rays. For AQ03, the centroid energy positions suggested the oxidation state of 2+ when plane C was oriented facing x-rays and a mixture of 2+ and 3+ when plane A was oriented facing x-rays.

The absorption edges of the samples and standards were determined from the peaks in the first derivative of XANES spectra as shown in Fig. 9 B. The absorption edges of Fe^0, Fe^{2+} and Fe^{3+} determined from Fe foil, FeO and Fe_2O_3 were 7112 eV, 7118 eV and 7126 eV, respectively. Those determined from the samples with plane C oriented facing x-rays were 7119.1 eV, 7119.3 eV and 7119.5 eV for AQ01, AQ02 and AQ03, respectively. Those with plane A oriented facing x-rays were 7120.9 eV for AQ01 and AQ02 and 7120.3 eV for AQ03. The obtained values were between those of the Fe^{2+} and Fe^{3+} standards suggesting a mixture of Fe^{2+} and Fe^{3+} in all samples. Similar to the result from the pre-edge fit, larger amount of Fe^{3+} was implied from the spectra measured with plane A oriented facing x-rays.

Therefore, for all samples, Fe could replace Al^{3+} in octahedral sites and possibly reside in interstitial sites but since 2+ ion is larger it is also possible that some Fe^{2+} also resides in channel sites which are larger sites. Together with the UV–Vis results, it could be inferred that most Fe ions resided in 6-fold coordinated sites, but some Fe^{2+} resided in channel sites which reduced the probability of finding IVCT between Fe^{2+} and Fe^{3+} in adjacent octahedral sites and hence the pale blue shades. The XAS result suggested a substantial amount of Fe^{2+} in AQ01. However, the intensity of the 373 and 428 nm peaks in the UV–Vis spectra of AQ01, which were assigned to Fe^{3+}, was similar to those of other samples. This suggested that the intensity of 373 and 428 nm

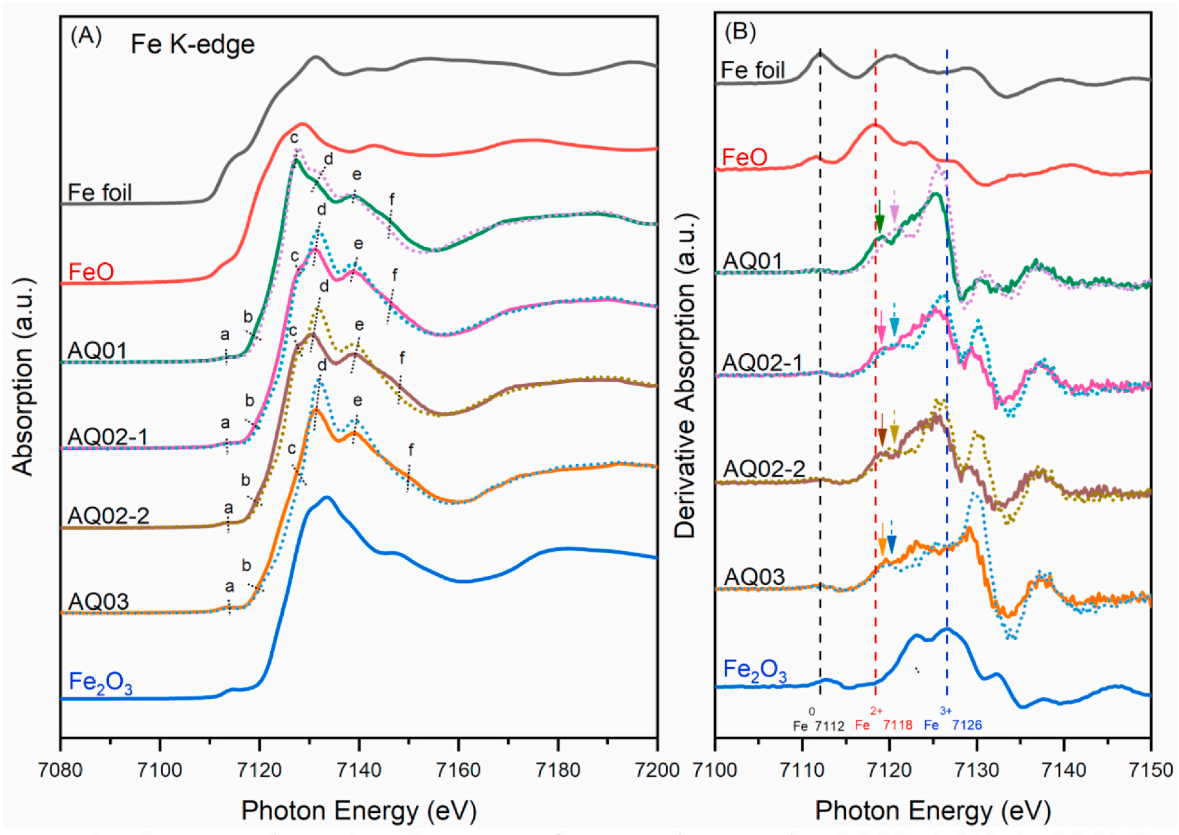

Fig. 9. Fe K-edge XANES spectra of aquamarine samples AQ01, AQ02-1, AQ02-2, AQ03, and standards; Fe foil, FeO and Fe_2O_3. XANES spectra corresponding to samples oriented with plane A facing x-rays are represented by dotted lines and those corresponding to plane C facing x-rays are represented by solid lines. (A) XANES spectra in energy scale with reference features including (**a**) pre-edge, (**b**) absorption-edge, and (**c**, **d**, **e**, **f**, **g**) features from multiple scattering phenomena. (B) The first derivative of XANES spectra of samples along with those of standards. The absorption edge energies are indicated by the arrows.

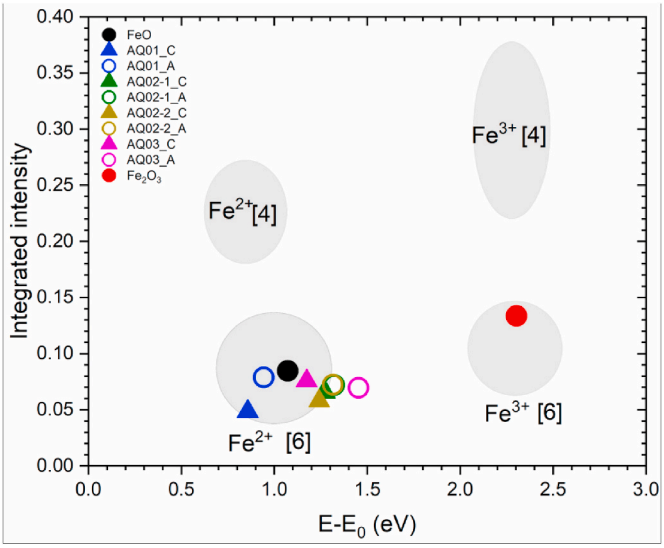

Fig. 10. Correlation between integrated pre-edge intensity and pre-edge centroid energy positions of aquamarine samples and oxide standards. Open circles correspond to spectra of samples with plane A oriented facing x-rays and those correspond to plane C oriented facing x-rays are represented by solid triangles. Shaded areas indicate typical parameters for four types of Fe species reported in Wilke et al. (2001). [4] represents a 4-fold coordinated Fe and [6] represents a 6-fold coordinated Fe. The uncertainties determined graphically from this plot are ± 0.2 eV in centroid position and ± 0.03 in integrated intensity.

peaks in the UV–Vis spectra was too small to reliably be used to imply the amount of Fe^{3+} in the samples.

The effect of x-ray dichroism for these samples could potentially lead to errors in data interpretation. The shift in absorption edge energy typically indicates a change in the oxidation state (Arcon et al., 1998), in this case however, the shift originated from orientation. Moreover, XANES features **c**, **d**, **e**, **f** were also shifted from 0.5 eV up to 2 eV. Therefore, careful sample alignment is crucial for XANES measurements of single crystal samples such as gemstones and uncertainties due to orientations should be considered.

3. Conclusions

Polarize scope was used to identify the c-axis of the samples and XRD were used to confirm the orientation of the polished face. The peak corresponding to the (100) plane of the beryl structure was identified when polished plane A was oriented facing x-rays and the peak corresponding to the (001) plane was identified when polished plane C was oriented facing x-rays. Raman spectra confirmed the beryl structure including predominant type-I H_2O in the structure. The NIR spectra agreed with Raman spectra although the technique was proved more sensitive to type-II H_2O in the structure as a small amount of type-II H_2O in the structure of AQ03 was detectable by NIR but not by Raman spectroscopy. Fe ions were investigated using UV–Vis and synchrotron XANES. The presence of Fe^{3+} in all samples was confirmed using UV–Vis spectra. Moreover, the UV–Vis spectra of AQ03 contained a peak shoulder at around 700 nm. This implied that there were both Fe^{3+} and Fe^{2+} in octahedral and interstitial sites of AQ03 which resulted in a deeper blue shade. The lack of peak shoulder at around

700 nm for AQ01 and AQ02 indicated that, for these samples, Fe^{2+} could instead reside in channel sites. This agreed with the postulation that a deep blue shade originated from IVCT between Fe^{3+} and Fe^{2+} in octahedral sites. The absorption edge positions and pre-edge centroid energy positions of XANES spectra confirmed the presence of both Fe^{3+} and Fe^{2+}. The pre-edge analysis indicated predominantly 6-fold coordinated Fe in all samples.

The effect of dichroism was observed in Raman spectroscopy, NIR, UV–Vis and XANES. For Raman spectroscopy, clearer Raman bands were observed when samples were oriented with plane A facing laser, especially the band at 1068 cm^{-1} corresponding to type-II H_2O molecules and deformation of O_2–Al/Be–O_2. The NIR and UV–Vis spectra measured from both orientations gave complementary information. Uncertainties of oxidation states in XANES measurements could be observed. It is thus crucial for XANES interpretation that dichroism should be considered and only data collected from samples oriented similarly could be compared.

CRediT authorship contribution statement

Nantharat Bunnag: Conceptualization, Investigation, Validation. **Bootsaba Kasri:** Investigation, Formal analysis. **Watcharakon Setwong:** Data curation, Visualization, Writing - original draft. **Ekkasit Sirisurawong:** Investigation, Validation. **Maneerat Chotsawat:** Visualization, Writing - original draft. **Prae Chirawatkul:** Writing - review & editing. **Chatree Saiyasombat:** Conceptualization, Supervision, Visualization, Writing - review & editing.

Declaration of competing interest

The authors declare that they have no known competing financial interests or personal relationships that could have appeared to influence the work reported in this paper.

Acknowledgements

This work was supported by Synchrotron Light Research Institute (Public Organization), SLRI, and the faculty of Gems, Burapha University, Chanthaburi campus. We would like to acknowledge the SLRI, for provision of beamtime at BL1.1W and laboratory equipment used in this work. And we also would like to thank the staff of BL1.1W for their assistance.

References

Adamo, I., Pavese, A., Prosperi, L., Diella, V., Ajò, D., Gatta, G.D., Smith, C.P., 2008. Aquamarine, Maxixe-type beryl, and hydrothermal synthetic blue beryl: analysis and identification. Gems Gemol. 44, 214–226.

Adams, D.M., Gardner, I.R., 1974. Single-crystal vibrational spectra of beryl and dioptase. J. Chem. Soc., Dalton Trans. 14, 1502–1505.

Arcon, I., Mirtic, B., Kodre, A., 1998. Determination of valence states of chromium in calcium chromates by using X-ray absorption near-edge structure (XANES) spectroscopy. J. Am. Ceram. Soc. 81 (1), 222–224.

Aurisicchio, C., Fioravanti, G., Grubessi, O., Zanazzi, P., 1988. Reappraisal of the crystal chemistry of beryl. Am. Mineral. 73 (7–8), 826–837.

Chankhantha, C., Thanasuthipitak, P., Kidkhunthod, P., 2016. Iron K-edge xanes study of heated green beryl from Madagascar. Walailak J. Sci. Technol. 13 (12), 977–983.

Charoy, B., De Donato, P., Barres, O., Pinto-Coelho, C., 1996. Channel occupancy in an alkali-poor beryl from Serra Branca (Goias, Brazil); spectroscopic characterization. Am. Mineral. 81 (3–4), 395–403.

Deer, W.A., Howie, R.A., Zussman, J., 1997. Rock-forming Minerals: Single-Chain Silicates 2A Geological Society of London.

Dyar, M.D., Gunter, M.E., Delaney, J.S., Lanzirotti, A., Sutton, S.R., 2002. Use of the spindle stage for orientation of single crystals for microXAS: isotropy and anisotropy in Fe-XANES spectra. Am. Mineral. 87 (10), 1500–1504.

Fritsch, E., Rossman, G.R., 1988. An update on color in gems. Part 2: colors involving multiple atoms and color centers. Gems Gemol. 24 (1), 3–15.

Goldman, S.D., Rossman, G.R., Parkin, K.M., 1978. Channel constituents in beryl. Phys. Chem. Miner. 3 (3), 225–235.

Hunt, G.R., Salisbury, J.W., 1970. Visible and near-infrared spectra of minerals and rocks : I silicate minerals. Mod. Geol. 1, 283–300.

Kim, Charles C., Bell, M.I., McKeown, D.A., 1995. Vibrational analysis of beryl (Be3Al2Si6O18) and its constituent ring (Si6O18). Phys. B Condens. Matter 205 (2), 193–208.

Nassau, K., Prescott, B.E., Wood, D.L., 1976. The deep blue Maxixe-type color center in beryl. Am. Mineral. 61 (1–2), 100–107.

O'Bannon, E., Williams, Q., 2016. Beryl-II, a high-pressure phase of beryl: Raman and luminescence spectroscopy to 16.4 GPa. Phys. Chem. Miner. 43 (9), 671–687.

Parkin, K.M., Loeffler, B.M., Burns, R.G., 1977. Mössbauer spectra of kyanite, aquamarine, and cordierite showing intervalence charge transfer. Phys. Chem. Miner. 1 (3), 301–311.

Prencipe, M., Nestola, F., 2007. Minerals at high pressure. Mechanics of compression from quantum mechanical calculations in a case study: the beryl (Al4Be6Si12O36). Phys. Chem. Miner. 34 (1), 37–52.

Sherriff, B., Grundy, H.D., Hartman, J., Hawthorne, F., Cerny, P., 1991. The incorporation of alkalis in beryl; a multinuclear MAS NMR and crystal-structure study. Can. Mineral. 29 (2), 271–285.

Spinolo, G., Fontana, I., Galli, A., 2007. Optical absorption spectra of Fe2+ and Fe3+ in beryl crystals. Phys. Status Solidi 244 (12), 4660–4668.

Taran, M.N., Rossman, G.R., 2001. Optical spectroscopic study of tuhualite and a re-examination of the beryl, cordierite, and osumilite spectra. Am. Mineral. 86 (9), 973–980.

Waychunas, G.A., Brown, G.E., Jackson, W., Ponader, C., 1989. In-situ high temperature x-ray absorption study of iron in alkali silicate melts and glasses. Phys. B Condens. Matter 158, 67–68.

Waychunas, G.A., Brown, G.E., 1990. Polarized X-ray absorption spectroscopy of metal ions in minerals. Phys. Chem. Miner. 17 (5), 420–430.

Wood, D.L., Nassau, K., 1968. The characterization of beryl and emerald by visible and infrared absorption spectroscopy. Am. Mineral.: Journal of Earth and Planetary Materials 53 (5–6), 777–800.

Wilke, M., Farges, F., Petit, P.E., Brown Jr., G.E., Martin, F., 2001. Oxidation state and coordination of Fe in minerals: an Fe K-XANES spectroscopic study. Am. Mineral. 86 (5–6), 714–730.

Wood, D.L., Nassau, K., 1967. Infrared spectra of foreign molecules in beryl. J. Chem. Phys. 47 (7), 2220–2228.

Zhukova, E.S., Torgashev, V.I., Gorshunov, B.P., Lebedev, V.V., Shakurov, G.m.S., Kremer, R.K., Pestrjakov, E.V., Thomas, V.G., Fursenko, D.A., Prokhorov, A.S., 2014. Vibrational states of a water molecule in a nano-cavity of beryl crystal lattice. J. Chem. Phys. 140 (22), 224317.